

A rotary frequency converter model for electromechanical transient studies of $16\frac{2}{3}$ Hz railway systems

John Laury^{a,1,*}, Lars Abrahamsson^a, Math H. J Bollen^a

^a*Luleå University of Technology, Electrical Power Engineering Group, Skellefteå, Sweden*

Abstract

Railway power systems operating at a nominal frequency below the frequency of the public grid (50 or 60 Hz) are special in many senses. One is that they exist in a just few countries around the world. However, for these countries such low frequency railways are a critical part of their infrastructure.

The number of published dynamic models as well as stability studies regarding low frequency railways is small, compared to corresponding publications regarding 50 Hz/60 Hz public grids. Since there are two main type of low frequency railways; synchronous and asynchronous, it makes the number of available useful publications even smaller. One important reason for this is the small share of such grids on a global scale, resulting in less research and development man hours spent on low frequency grids.

This work presents an open model of a (synchronous-synchronous) rotary frequency converter for electromechanical stability studies in the phasor

*Corresponding author

Email address: `john.laury@ltu.se` (John Laury)

¹The financial support for this project from the Swedish Transport Administration is greatly acknowledged.

domain, based on established synchronous machine models. The proposed model is designed such that it can be used with the available data for a rotary frequency converter.

The behaviour of the model is shown through numerical electromechanical transient stability simulations of two example cases, where a fault is cleared, and the subsequent oscillations are shown. The first example is a single-fed catenary section and the second is doubly-fed catenary section.

Keywords: Low Frequency Railways, $16\frac{2}{3}$ Hz, Modelling, Simulations, Transient Stability, Rotary Frequency Converter, Motor Generator set, Multi machine system.

1. Introduction

Low-frequency AC railways exist only in six countries: Austria, Germany, Switzerland, Norway, Sweden and in the (North East of the) U.S. [1, 2]. As the frequency in the railway is different from the public grid, frequency conversion is needed [2, 3]. The conversion can be done by using Motor-Generator sets, also called Rotary Frequency Converter (RFC).

Such an RFC consists of a three-phase motor and a single-phase synchronous generator mounted on the same mechanical shaft.

In Austria, Germany and Switzerland a double-fed induction motor is used, allowing active power to be controlled [2, 3, 4]. The active power supplied by the RFCs follows an active-power-frequency droop characteristic [4].

In Sweden, Norway and the North Eastern U.S. the motor is of synchronous type and therefore the railway grid is synchronous to the three-

phase public grid. Active power through an RFC with synchronous motor is dependent on the angle difference between the three-phase public grid and the single-phase low-frequency railway grid of $16\frac{2}{3}$ Hz (Sweden, Norway) or 25 Hz (North Eastern U.S.) at the RFC locations.

A very limited amount of previous published work has been done on electromechanical stability of low-frequency railways that are synchronous with the public grid.

Small-signal studies on the Norwegian synchronous low-frequency railway grid have been performed in [5, 6, 7, 8]. It was found from those studies that one of the most commonly used RFCs has a poorly damped eigenfrequency that could be excited by modern locomotives, which could lead to system instability. Those studies either use the classical model (which is essentially a constant electromotive force (emf) behind a transient reactance) for each of the two synchronous machines, or the commercial software Simpow for simulations with higher order synchronous machine models.

In [9] a transient stability assessment is done for the low-frequency railway grid of the North Eastern U.S. No models of RFC were presented in that study as the commercial software PSLF from GE was used.

Reference [10] uses the classical model of a synchronous machine to investigate the transient stability of the Northern part of the Swedish railway system in the end of the 1980's.

There are only a small number of commercial software packages available that simulate dynamics of low-frequency railways that are synchronously connected to the public grid. Furthermore the models used in such software are not published. Thus, complete electromechanical model descriptions of

RFCs as part of low-frequency railway grids is non-existent in the literature.

With increased traffic and with more advanced train control, there is a need for stability studies to increase the understanding of low-frequency railway grids under different scenarios, such as faults or the impact of different control systems. Therefore, there is an identified need for an open dynamic model of an RFC that can be used for transient stability studies. An open, transparent model allows research and education (gathering and spreading of knowledge) on the stability of the mentioned railway without being depended on specialized commercial software packages.

The aim of this paper is to present a high order synchronous-synchronous RFC model that can be used for transient stability studies. The established 6:th order Andersson-Fouad synchronous machine model [11, 12, 13] is used to describe the dynamics of motor and generator of an RFC. The behaviour of the RFC model is shown in two transient stability studies: a study in which only one RFC is feeding a catenary section (single feeding mode); and a study in which two RFCs are feeding the a catenary section (interconnected mode). The studied results give an insight in the transient stability of synchronously connected low-frequency railway grids.

The remainder of this paper is organised as follows: Section 2 presents both steady state and the proposed dynamical model of an RFC. Section 3 presents the interfacing of the dynamic RFC machine model to the static grid model for performing the intended electromechanical transient stability studies. The electromechanical transient stability case studies using the proposed RFC model from Section 2 and 3 are presented in Section 4. The results are presented in Section 5 and in Section 6 the conclusions are summarized.

2. RFC model

The motors and the generators of the RFCs in the Norwegian and Swedish low-frequency railway grids of $16\frac{2}{3}$ Hz are all salient pole synchronous machines [10, 14]. The three-phase motor has $p^m \in 2 \cdot \mathbb{N}$ magnetic poles, whereas the single-phase generator has $p^g = \frac{p^m}{3} \in 2 \cdot \mathbb{N}$ magnetic poles. Thus, it is needed that $p^m \in 6 \cdot \mathbb{N}$ magnetic poles. The result is that the electrical frequency induced in the stator of the single-phase generator is exactly one third of the frequency in the three-phase public grid of 50 Hz in steady state, that is $16\frac{2}{3}$ Hz.

Since the models work in per-unit angular frequencies, the exact number of poles in the machines is not of relevance for the computations, but in the Scandinavian system the motors have 12 poles (6 pole pairs), and the generators have 4 poles (2 pole pairs) [14].

2.1. Steady-state model

From electrical machine theory [11, 15] it is known that the load angle of a salient pole machine

$$\delta = \arctan \left(\frac{X_q P_{\blacksquare}}{|U|^2 + X_q Q_{\blacksquare}} \right) \quad (1)$$

where X_q , P_{\blacksquare} , $|U|$ and Q_{\blacksquare} are the quadrature reactance, generated/consumed active power, terminal voltage magnitude and generated/consumed reactive power in p.u., respectively. The subscript \blacksquare is used to make Equation (1) a generalized expression for motors as well as generators. The load angle defined as in Equation (1) is valid under the assumption that the machine resistance is neglected, which is justified by the fact that the resistance is

much smaller than the reactance. In the remainder of this paper, it is for simplicity assumed that the RFCs are lossless.

When an RFC is loaded on the railway grid (generator) side, the total resulting negative (confer Equation (9)) voltage phase angle shift between the points of common connection of the motor and the generator is the sum of the load angles of the motor and the generator. The voltage phase shift expressed in $16\frac{2}{3}$ Hz angles

$$\psi = \frac{1}{3} \arctan \left(\frac{-X_q^m \cdot P_G^m}{|U^m|^2 - X_q^m Q_G^m} \right) + \arctan \left(\frac{X_q^g \cdot P_G^g}{|U^g|^2 + X_q^g Q_G^g} \right), \quad (2)$$

where the superscripts m and g stands for motor and generator, respectively.

Positive active power demand on the railway side results in the generated active power of the RFC generator,

$$P_G^g > 0, \quad (3)$$

which means that the generator operates in generator mode. At the same time, the generated active power of the RFC motor

$$P_G^m < 0, \quad (4)$$

which means that the motor operates in motor mode. With the assumption that the RFC is lossless,

$$-P_G^m = P_G^g \quad (5)$$

holds.

For the simplicity of modelling, the step-down transformer leakage reactance of the motor X_T^m (confer Table 1) is added to X_q^m in order to redefine X_q^m according to,

$$X_q^m := X_T^m + X_q^m, \quad (6)$$

and the step-up transformer leakage reactance X_T^g of the generator is added to X_q^g in order to form a new redefined X_q^g in the same way as Equation (6) for the motor.

As active power flows from the public grid to the railway grid, the terminal angle of the single-phase generator will fall relative to the angle θ_{50}^m on the three-phase grid to which the motor is connected. This angle drop takes place in two steps; first

$$\delta_m = \frac{\theta_{50}^m}{3} - \frac{1}{3} \arctan \left(\frac{-X_q^m \cdot P_G^m}{|U^m|^2 - X_q^m Q_G^m} \right), \quad (7)$$

and secondly

$$\theta^g = \delta_m - \arctan \left(\frac{X_q^g \cdot P_G^g}{|U^g|^2 + X_q^g Q_G^g} \right), \quad (8)$$

where δ_m denotes the per-unit mechanical angle of Equation (34). The angle δ_m also represents the electrical angle of the RFC's rotor expressed in the $16\frac{2}{3}$ Hz grid frame. Therefore, putting Equations (2), (7) and (8) together, the terminal angle of the generator

$$\theta^g = \frac{\theta_{50}^m}{3} - \psi. \quad (9)$$

At the railway grid side, the voltage magnitude $|U^g|$ after the step-up transformer is controlled as

$$|U^g| = U_0 - K_U Q_G^g, \quad (10)$$

where U_0 is the no-load voltage. In addition, K_U in Equation (10) is a droop coefficient which is scaled to the RFC single-phase generator rating. The use of such a scaled droop coefficient K_U results in reactive load sharing between the different active RFCs in a converter station [16].

On the three-phase side; there are according to [17] three control options:

1. the terminal voltage at the bus of common connection is controlled to a constant value,
2. the reactive power of the motor is controlled to a constant value, or
3. the power factor of the motor is controlled to a constant value,i

that can be used. Since the models proposed and applied in this paper assumes an infinite bus connecting to the motors, the resulting control in steady-state will in practice be both options 1 and 2 in the list above, with voltage U^m controlled to 1 p.u. and reactive power Q_G^m controlled to 0 p.u. Dynamically, however, none such control takes place, since it is not needed. During the transient, the reactive power of the motor will fluctuate a bit until it stabilizes at 0 again.

2.2. Dynamic model

2.2.1. The mechanical equations

The mechanical shaft to which one RFC's both synchronous machines are mounted on is assumed to be mechanically stiff. That assumption implies that the rotors of both machines in one RFC rotate at the same speed. The load torque of the synchronous motor is the input to the synchronous generator. This results in the swing equation of an RFC to be

$$(J^m + J^g) \frac{d\omega_m(t)}{dt} = T^m(t) - T^g(t), \quad (11)$$

where J^m and J^g denote the moments of inertia of motor and generator, respectively. Moreover, ω_m stands for the mechanical angular frequency, whereas T^m and T^g stand for the electromagnetic air gap torques of motor and generator, respectively.

The electrical part of the machine model proposed in this paper and presented in Section 2.2.2, includes the effects of damper windings. Mechanical damping caused by windage and friction is assumed to be small and is therefore neglected.

A synchronously rotating reference frame with a constant mechanical angular frequency, ω_{sm} , is chosen as angular reference, so that the mechanical rotor angle (that is, the angular displacement of the rotor with respect to a stationary axis on the stator),

$$\beta_m(t) = \omega_{sm}t + \delta_m(t), \quad (12)$$

where $\delta_m(t)$ is the angular position with respect to the chosen synchronously rotating reference frame ω_{sm} . The velocity (that is, the angular frequency) of the rotor (confer to Equation (11)),

$$\omega_m(t) = \frac{d\beta_m(t)}{dt} = \omega_{sm} + \frac{d\delta_m(t)}{dt}, \quad (13)$$

relative to the synchronously rotating reference frame. In addition, the acceleration of the mechanical rotor angle

$$\frac{d^2\beta_m(t)}{dt^2} = \frac{d^2\delta_m(t)}{dt^2}. \quad (14)$$

The total moment of inertia of the RFC,

$$J^{mg} = J^m + J^g \quad (15)$$

and J^{mg} as expressed in terms of the per unit inertia constant H^{mg} becomes

$$J^{mg} = \frac{2H^{mg}S_B}{\omega_{sm}^2}. \quad (16)$$

In Equation (16), S_B denotes the base power used and S_B is numerically defined in Table 2. Inserting Equation (16) in Equation (11) and multiplying with the mechanical angular speed yields

$$\omega_m(t) \frac{2H^{mg} S_B}{\omega_{sm}^2} \frac{d\omega_m(t)}{dt} = \omega_m(t) (T^m(t) - T^g(t)). \quad (17)$$

Reformulating Equation (17) and expressing it in p.u. results in

$$2H^{mg} \omega_{p.u.}(t) \frac{d\omega_{p.u.}(t)}{dt} = -P_{p.u.}^m(t) - P_{p.u.}^g(t). \quad (18)$$

Moreover, Equations (13) and (18) can be transformed to the state space form,

$$\frac{d\delta_m(t)}{dt} = \Delta\omega_{p.u.}(t) \omega_{sm} \quad (19)$$

$$\frac{d\omega(t)_{p.u.}}{dt} = \frac{1}{2H^{mg} \omega(t)_{p.u.}} (-P_{p.u.}^m(t) - P_{p.u.}^g(t)), \quad (20)$$

where

$$\Delta\omega_{p.u.}(t) = \omega_{p.u.}(t) - 1 \quad (21)$$

is the speed deviation of the rotor from the synchronously rotating reference frame, ω_{sm} .

Note that the torque of a motor is defined positive for consumption, whereas the torque of a generator is defined positive for generation. Since this paper consequently treats all machine powers as generated powers, the positive motor torque in Equation (17) multiplied by the mechanical angular frequency $\omega_m(t)$ becomes a negatively signed power, that is $-P_{p.u.}^m(t)$, in Equations (18) and (20). The air gap powers in Equations (18) and (20) generated in the motor

$$P_{p.u.}^m(t) = P_G^m(t), \quad (22)$$

and the generator

$$P_{\text{p.u.}}^g(t) = P_G^g(t), \quad (23)$$

respectively, because of the assumption of lossless machines. The mechanical rotor angle (to be stringent; the angular position with respect to ω_{sm}), δ_m , is multiplied by the number of pole pairs $\frac{p^g}{2}$ and $\frac{p^m}{2}$ to obtain the electrical rotor angle in the $16\frac{2}{3}$ Hz and the 50 Hz electrical frames, respectively.

2.2.2. The electrical equations

The 6:th order Andersson-Fouad model [11, 12, 13] of a synchronous machine is used to describe the links between stator fluxes, stator currents and field voltages. Such a machine model considers the dynamics of the damper windings and is suitable to be used for stability studies [13]. For simplicity magnetic saturation is neglected.

The time derivative of the transient emf in the direct axis

$$\dot{E}'_d = -E'_d - I_q(X_q - X'_q), \quad (24)$$

however, the synchronous machines are of salient pole type, which implies that

$$X'_q = X_q \quad (25)$$

according to [11, Table 4.2]. Since \dot{E}'_d is equal to zero in steady-state, Equations (24) and (25) give that $E'_d = 0$ for motor as well as generator in a Scandinavian RFC. In turn, the 6:th order model of [11, Section 11.1.7.1] collapses to the 5:th order model of [11, Section 11.1.7.2]. Note, that all variables henceforth are expressed in the p.u. system, unless otherwise stated. Therefore, the p.u. subscripts are omitted henceforth.

The resulting electrical equations of an RFC are:

$$T_{do}^m \dot{E}_q^m = E_f^m - E_q^m + I_d^m (X_d^m - X_d'^m) \quad (26)$$

$$T_{do}^{''m} \dot{E}_q^{''m} = E_q^m - E_q^{''m} + I_d^m (X_d'^m - X_d^{''m}) \quad (27)$$

$$\begin{aligned} T_{qo}^{''m} \dot{E}_d^{''m} &= -E_d^{''m} - I_q^m (X_q'^m - X_q^{''m}) = \\ &= \{\text{Equation (25)}\} = \\ &= -E_d^{''m} - I_q^m (X_q^m - X_q^{''m}) \end{aligned} \quad (28)$$

$$T_{do}^g \dot{E}_q^g = E_f^g - E_q^g + I_d^g (X_d^g - X_d'^g) \quad (29)$$

$$T_{do}^{''g} \dot{E}_q^{''g} = E_q^g - E_q^{''g} + I_d^g (X_d'^g - X_d^{''g}) \quad (30)$$

$$\begin{aligned} T_{qo}^{''g} \dot{E}_d^{''g} &= -E_d^{''g} - I_q^g (X_q'^g - X_q^{''g}) = \\ &= \{\text{Equation (25)}\} = \\ &= -E_d^{''g} - I_q^g (X_q^g - X_q^{''g}) \end{aligned} \quad (31)$$

where T_{do}' is the direct-axis transient open circuit time constant. The sub-transient open circuit time constant in the quadrature and the direct axes are T_{qo}'' and T_{do}'' , respectively. The transient voltage in the quadrature axis is E_q' , whereas the sub-transient voltage in the direct and the quadrature axes are E_d'' and E_q'' . The steady-state, transient and sub-transient reactances in the direct-axis are X_d , X_d' and X_d'' , respectively. The steady-state, transient and sub-transient reactances in the quadrature-axis are X_q , X_q' and X_q'' , respectively, but since salient pole machines are used Equation (25) still holds.

The air-gap powers of both synchronous machines of an RFC are:

$$P^m = E_d^{''m} I_d^m + E_q^{''m} I_q^m + (X_d^{''m} - X_q^{''m}) I_d^m I_q^m \quad (32)$$

$$P^g = E_d^{''g} I_d^g + E_q^{''g} I_q^g + (X_d^{''g} - X_q^{''g}) I_d^g I_q^g. \quad (33)$$

2.2.3. *Dynamic RFC model*

With Equations (19), (20) and (26) to (33), a total of eight first order differential equations and two algebraic equations are obtained to describe the dynamics of an RFC excluding the excitation system model. There are 8 differential equations since 2 machines with 5:th order models are considered, but they share the mechanical properties in Equations (19) and (20) ($5+5-2 = 8$).

2.2.4. *Excitation system*

To control the voltage magnitude after the step-up transformer on the railway side, the RFC generator is equipped with an excitation system. The inputs are the calculated voltage magnitude reference $|U|^{\text{ref}}$ and the measured voltage magnitude $|U^g|$. Deviation from the calculated voltage reference value causes that the excitation system to adjust the field voltage E_f^g of the RFC generator.

On the motor side, the voltage magnitude or reactive power is controlled to a constant reference value. If there is a deviation from the reference value, the excitation system of the motor will adjust the field voltage E_f^m .

For modelling purpose, any of the standard models of excitation systems from [18] can be used on the RFCs motor and generator, respectively.

3. **Model for electromechanical transient stability studies**

The stator voltages of each machine are expressed in their own dq rotating reference frame for that machine. This reference rotates independently from other machines of the system.

The electrical equations of the three phase public grid are expressed in a common 50 Hz Re-Im reference frame. The subscript a_{50} and b_{50} stands for real and imaginary part of that reference frame, respectively. The electrical equations of the railway grid are also expressed in common Re-Im reference frame, but rotating at $16\frac{2}{3}$ Hz. The subscript $a_{16\frac{2}{3}}$ and $b_{16\frac{2}{3}}$ stands for the real and imaginary part of that frame.

The transformation matrix \mathbf{T} is used to transform the motor and generator stator quantities from a 50 Hz or $16\frac{2}{3}$ Hz reference frame to the rotor reference frame of the particular RFCs motor and generator, respectively. The transformation matrix,

$$\mathbf{T} = \begin{bmatrix} -\sin(\frac{p}{2}\delta_m) & \cos(\frac{p}{2}\delta_m) \\ \cos(\frac{p}{2}\delta_m) & \sin(\frac{p}{2}\delta_m) \end{bmatrix} \quad (34)$$

where p is the number of poles of the particular machine considered. Note that \mathbf{T} is orthogonal and the same matrix is used for backward and forward transformations.

If $p = p_g$ in Equation (34) the transformation matrix \mathbf{T} is denoted as \mathbf{T}^g , and used to transform the dq rotor variables of the generator to the $16\frac{2}{3}$ Hz frame of the railway grid and the other way around. The transformation matrix \mathbf{T} is denoted as \mathbf{T}^m if $p = p_m$, and used to transform the dq rotor variables of the motor to the 50 Hz reference frame.

Consider a synchronous railway system as shown in Figure 1. All RFCs motor are connected to infinite buses, where the voltage U_{50} is set to one p.u. and the voltage phase angle θ_{50} is set zero and is constant. This assumption is justified as several connection points in the public grid where the RFC are connected to are strong. The i :th RFC motor is then implemented as

a voltage source $\bar{E}_i''^m = E_{d,i}''^m + jE_{q,i}''^m$ in the dq rotor reference frame of the motor.

On the railway side, the i :th RFC generator is connected to the railway grid as an equivalent Norton current source, $\bar{I}_{N,i}^g$. The voltages $E_{d,i}''^g$ and $E_{q,i}''^g$ of the i :th RFC generator are transformed from the dq reference of generator into the $16\frac{2}{3}$ Hz reference frame, and in that frame the injected Norton current is calculated according to

$$\begin{bmatrix} E_{a,i_{16\frac{2}{3}}}''^g \\ E_{b,i_{16\frac{2}{3}}}''^g \end{bmatrix} = \mathbf{T}_i^g \begin{bmatrix} E_{d,i}''^g \\ E_{q,i}''^g \end{bmatrix} \quad (35)$$

$$\bar{I}_{N,i}^g = \frac{E_{a,i_{16\frac{2}{3}}}''^g + jE_{b,i_{16\frac{2}{3}}}''^g}{jX_{d,i}''^g} \quad (36)$$

According to [11, 19], the effects of sub-transient saliency are normally small and can therefore be neglected, with the assumption that $X_d'' \approx X_q''$. As seen in 1 the approximation is acceptable for the single phase-generator, whereas for the three-phase motor the approximation is not acceptable as there is to large difference between X_d'' and X_q'' . However, to avoid the need of iterative computation for handling saliency and for fast simulations, X_d'' is set equal to X_q'' for both machines. This assumption affects Equations (32) and (33).

To connect the RFCs' generators to the railway grid for the simulations, the admittance matrix $\mathbf{Y}_{bus,16\frac{2}{3}}$ describing the railway grid is augmented to $\mathbf{Y}_{bus,16\frac{2}{3}}^{aug}$. The augmentation is done by adding the sub-transient reactances as shunt admittances to the $\mathbf{Y}_{bus,16\frac{2}{3}}$ matrix where the RFC generators are connected to the railway grid. For simplicity, the loads are modelled as shunt admittances and are added to in a similar way to the $\mathbf{Y}_{bus,16\frac{2}{3}}$ matrix.

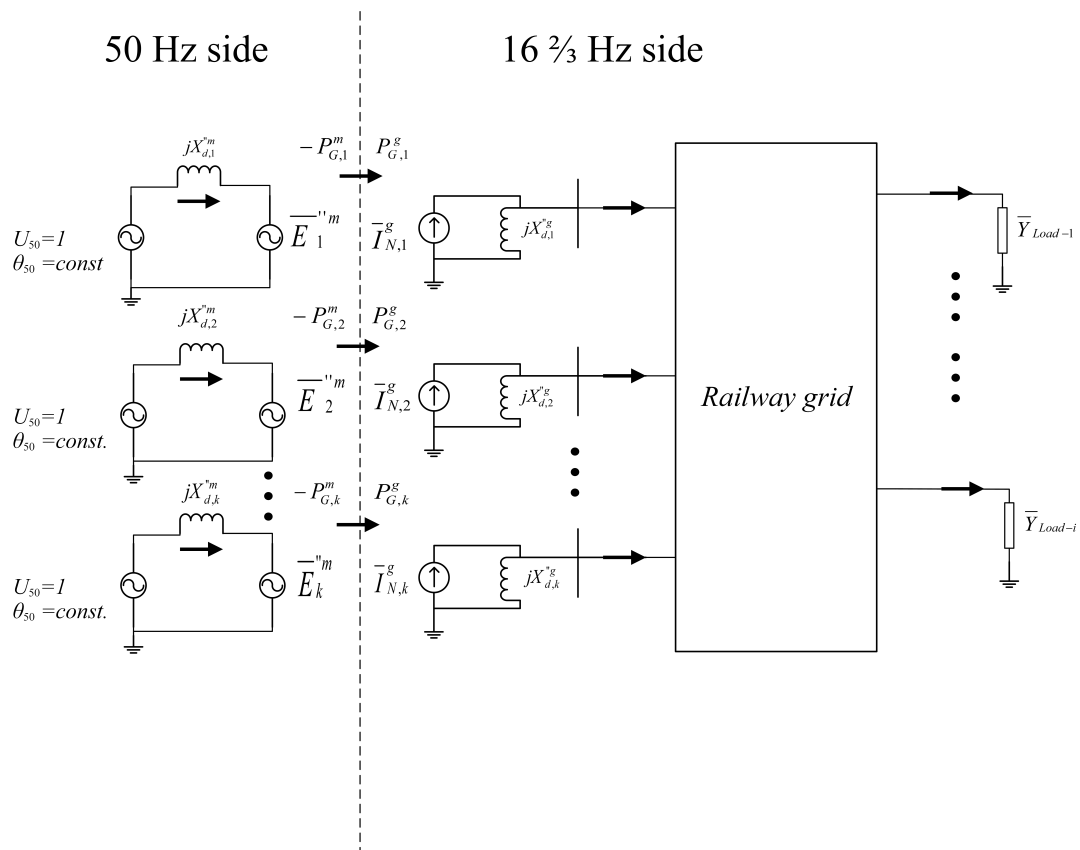


Figure 1: Model setup of a synchronous-synchronous railway system for $i = 1 \dots k$ RFCs.

As $X_d'' = X_q''$ for both of the RFC machines and loads are expressed as admittances, a linear load flow is used. The voltages of the railway grid are calculated in the $16\frac{2}{3}$ Hz common Re-Im phasor frame as:

$$U_{16\frac{2}{3}} = (Y_{bus,16\frac{2}{3}}^{aug})^{-1} I_N^g. \quad (37)$$

Solving Equations (19), (20), (26) to (33) and (37), the current of the i :th RFCs generator and motor in the dq frame, respectively is

$$\begin{bmatrix} I_{d,i}^g \\ I_{q,i}^g \end{bmatrix} = \frac{1}{X_{d,i}''^g} \begin{bmatrix} U_{q,i}^g - E_{q,i}''^g \\ -U_{d,i}^g + E_{d,i}''^g \end{bmatrix} \quad (38)$$

$$\begin{bmatrix} I_{d,i}^m \\ I_{q,i}^m \end{bmatrix} = \frac{1}{X_{d,i}''^m} \begin{bmatrix} U_{q,i}^m - E_{q,i}''^m \\ -U_{d,i}^m + E_{d,i}''^m \end{bmatrix}. \quad (39)$$

Active and reactive power injected by the i :th generator of the RFC into the railway grid is computed as:

$$P_i^g = U_{d,i}^g I_{d,i}^g + U_{q,i}^g I_{q,i}^g \quad (40)$$

$$Q_i^g = U_{d,i}^g I_{q,i}^g - U_{q,i}^g I_{d,i}^g \quad (41)$$

Active and reactive power of the motor injected by the i :th motor of the RFC into the 50 Hz grid is computed as:

$$P_i^m = U_{d,i}^m I_{d,i}^m + U_{q,i}^m I_{q,i}^m \quad (42)$$

$$Q_i^m = U_{d,i}^m I_{q,i}^m - U_{q,i}^m I_{d,i}^m. \quad (43)$$

The computational structure of i :th RFC connected to both the railway grid and public grid is shown in Figure 2.

The electrical rotor angles of the motors are referred to the constant 50 Hz angle θ_{50} of the infinite bus. The electrical rotor angles of the generators

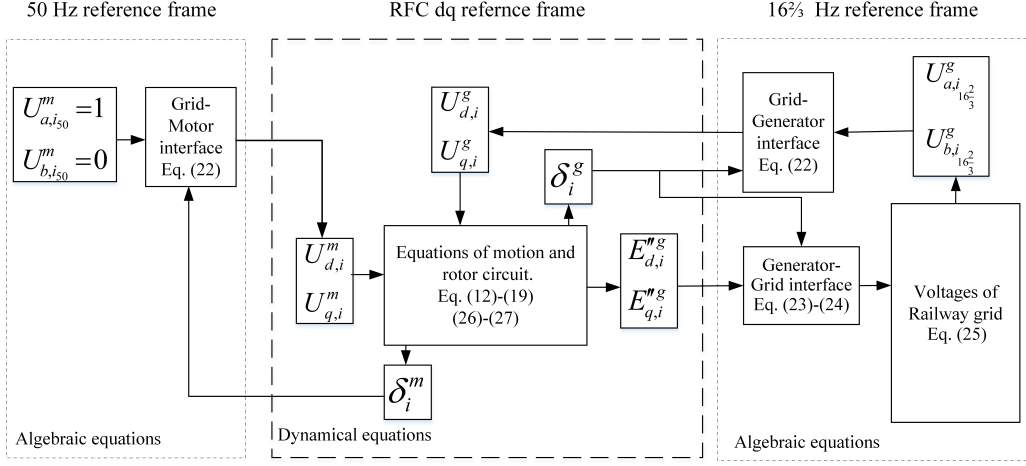


Figure 2: Model structure of the i -th RFC connected to both public grid and railway grid.

in interconnected mode can be referred to any of the other RFC generator on the railway grid side or the angle of the 50 Hz side.

3.1. Modelling discussion

In the overall modelling, transients associated with power/current flows in the railway grid and the public grid are assumed to have a fast decay time, so that a QSS (Quasi Steady-State) [20, 21] approach is used. As grid transients are neglected, the stator transients of the RFC machines have to be neglected [22, 11].

The negligence of stator transient introduces a conservatism to the model, as rotor speed deviation is increased [22]. One should however proceed with care regarding the implications of this negligence for RFC-fed synchronously operated (single-phase) low frequency railway grids, since so many operating conditions differ from public transmission grids fed by thermal or hydro-power generators. For example, the mechanic power of the generator shaft

is provided by another synchronous machine for synchronous-synchronous railway systems.

As recommended in [11, 22], also the rotor speed deviations are neglected in the stator equations. According to [22], this is not mainly done to make computations faster, but rather to counterbalance the effect of stator transients being neglected, considering the low-frequency rotor oscillations.

4. Cases studies

To investigate and characterize the behaviour of RFC model dynamics under a fault in the railway grid, the following cases have been studied

- Case 1: A single RFC feeding a catenary section (Single feeding mode), see Figure 3, is simulated to understand the dynamic behaviour of an RFC by itself.
- Case 2: Two RFCs feeding a catenary section (Interconnected mode), see Figure 4, are simulated to understand the dynamic interactions between a pair RFCs, one in each converter station.

The systems are investigated during no-load situation to avoid influence from the load. The system is disturbed by applying a balanced fault at 10 km from RFC 1. The fault is initiated at 1.8 seconds and cleared after 200 ms.

One of the most common RFC types used in Sweden is Q48/Q49. This type of RFC has been chosen for the studies to investigate the RFC model behaviour. Data about Q48/Q49 is given in Table 1. An equivalent impedance of the Booster Transformer (BT) catenary based on [23] is used, see Table 2.

The pre-fault conditions are obtained by a load flow calculation using parts of the software Train Power System Simulator (TPSS) presented in [24]. TPSS uses GAMS [25] and MatLab to model and solve load flows in phasor domain for low-frequency railway power systems synchronously connected to the public grid.

$X_q^m, X_d^m, X_d'^m, X_q''^m, X_d''^m$	0.49, 1.02, 0.3, 0.3, 0.21 [p.u.]
$T_{do}^m, T_{do}''^m, T_{qo}''^m$	3.6, 0.04, 0.09 [s]
Inertia constant motor, H_M	1.06 [MWs/MVA]
Rated power motor	10.7 [MVA]
Transformer ratio motor	80 [kV]/6.3 [kV]
Transformer leakage reactance of the motor, X_T^m	7.9%
$X_q^g, X_d^g, X_d'^g, X_q''^g, X_d''^g$	0.53, 1.39, 0.16, 0.10, 0.12 [p.u.]
$T_{do}^g, T_{do}''^g, T_{qo}''^g$	11.2, 0.07, 4 [s]
Inertia constant generator, H_G	1.14 [MWs/MVA]
Rated power generator	10 [MVA]
Transformer ratio generator	5.2 [kV]/17 [kV]
Transformer leakage reactance of the generator, X_T^g	4.2%

Table 1: RFC parameters of the Q48/Q49.

Due to the connection to the infinite bus, the excitation system on the motor has not been implemented and field voltages of the motors are kept constant. The majority of the RFC generators and motors in the Swedish rail-

Catenary impedance	$0.2+j0.2 \text{ } [\Omega/\text{km}]$
Base power, S_B	10 [MVA]
Base voltage railway side, U_B	16.5 [kV]
Base voltage 50 Hz side, U_{B50}	6.3 [kV]

Table 2: System parameters.

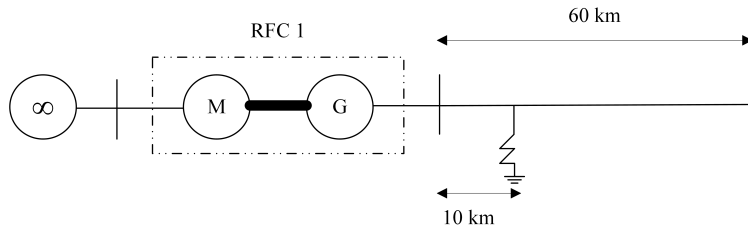


Figure 3: Case 1: Single feeding mode.

way system are equipped with brushless excitation systems. The AC5A [18] excitation model of such an excitation system provided by MatLab Simulink has been used.

The model presented of an RFC in Section 2 and its interface to the public grid and the railway grid represented in Section 3 has been implemented and simulated in MatLab Simulink, where the RFC dynamics and the electrical networks equations are solved. The fixed step solver *ode4* (Runge-Kutta algorithm) is used, with a step size equal to 1 ms.

Oscillation frequencies of various power system variables are determined for both of the cases described above in this section. Oscillation frequencies are presented together with other important simulation results in Section 5. An oscillation frequency is a simple measure to quantify a dynamic behaviour

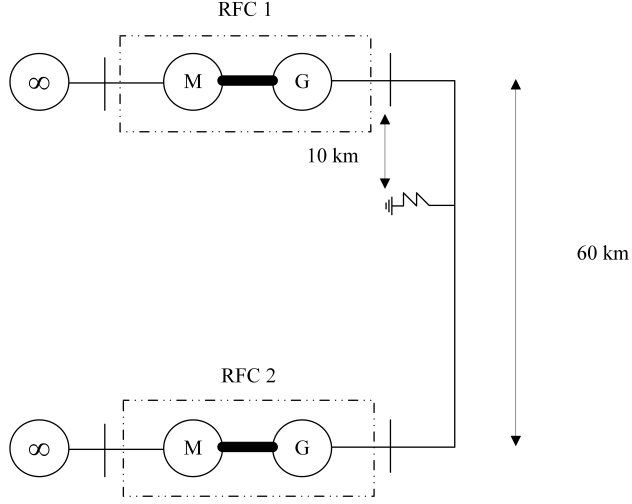


Figure 4: Case 2: Interconnected mode.

of a machine, an other component, or a system as a whole. By studying oscillation frequencies, one may get a rough picture of RFC and power system transient behaviour.

To estimate the average frequency of an oscillation, an average of four to ten consecutive estimated values of the oscillation frequency f_{osc} is used. The oscillation frequency f_{osc} between two peaks of a graph obtained from the simulations,

$$f_{osc} \approx \frac{1}{\Delta t}, \quad (44)$$

where Δt is the time difference between the peaks of the graph. The peaks are found by using the *Peak Finder* tool in MatLab Simulink.

5. Results

5.1. Case 1

At fault initiation, the voltage at the railway side drops to approximately 0.40 p.u. and decays further during the fault, see Figure 5. The impedance seen from the RFC to the fault location has an X/R ratio equal to one. Therefore the RFC generator will supply both active and reactive power during the fault. As active power increases suddenly at fault initiation, the RFC motor will see an increase in load. However, due to the inertia of the RFC machine the rotor speed and the three-phase active power will increase gradually as seen in Figures 6 and 7.

Based on the simulations, the average rotor oscillations is 1.96 Hz. The three-phase power of the motor and rotor angle oscillates with the same frequency against the 50 Hz grid. This type of oscillations can be expected for single synchronous machine at a power station which swing against a large power system according to [26, 27]. On the single phase side, as there is no other machines or infinite bus, the induced voltage vector of the RFC generator and the railway grid voltage vector have the same speed.

In Figure 8, the relative rotor angle is plotted against time and rotor speed oscillation. Both relative angle and rotor speed oscillation goes to zero, showing that the system is stable.

5.2. Case 2

During the fault, the rotor speed of RFC 1 drops more than the speed of RFC 2, as the fault current provided by RFC 1 generator is higher than RFC 2, see Figure 9c.

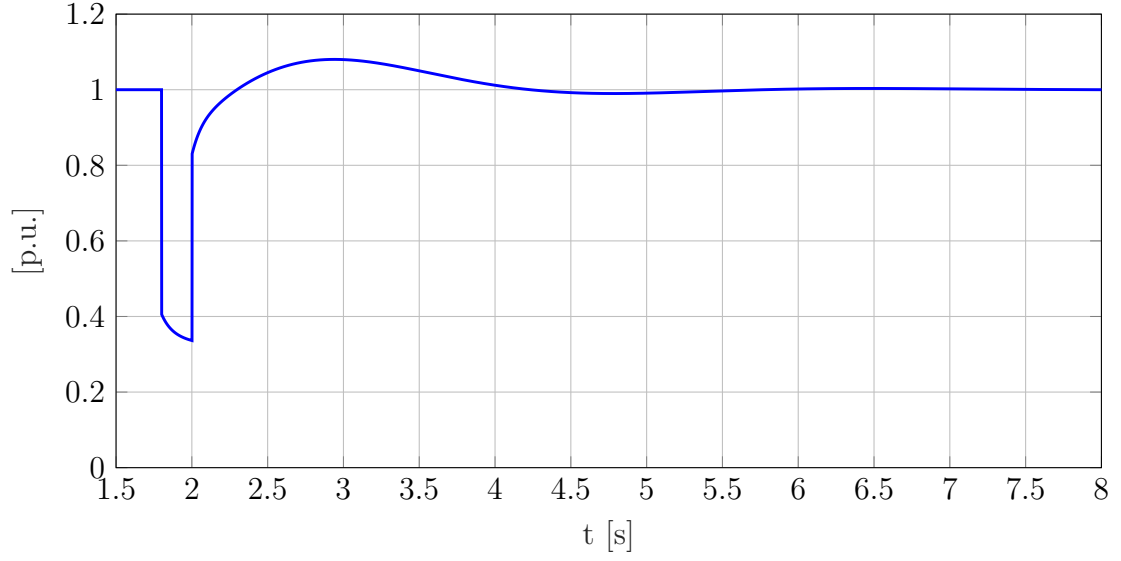


Figure 5: Voltage after the step-up transformer, railway side, Case 1.

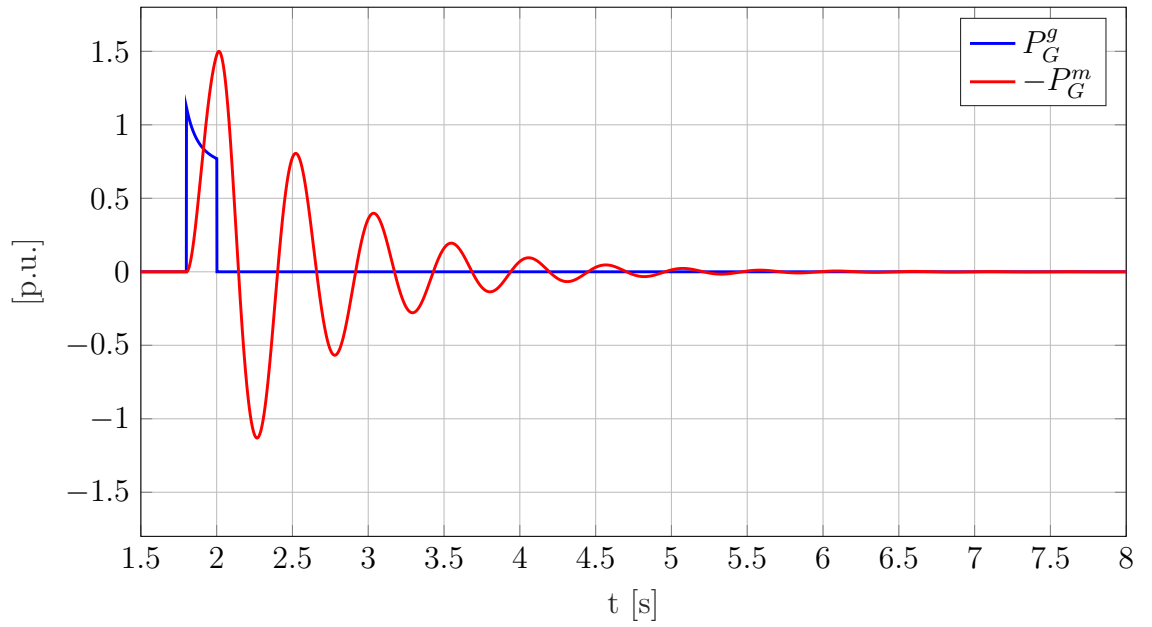


Figure 6: Generated (P_G^g) vs consumed ($-P_G^m$) active power of the RFC generator and motor, respectively, Case 1.

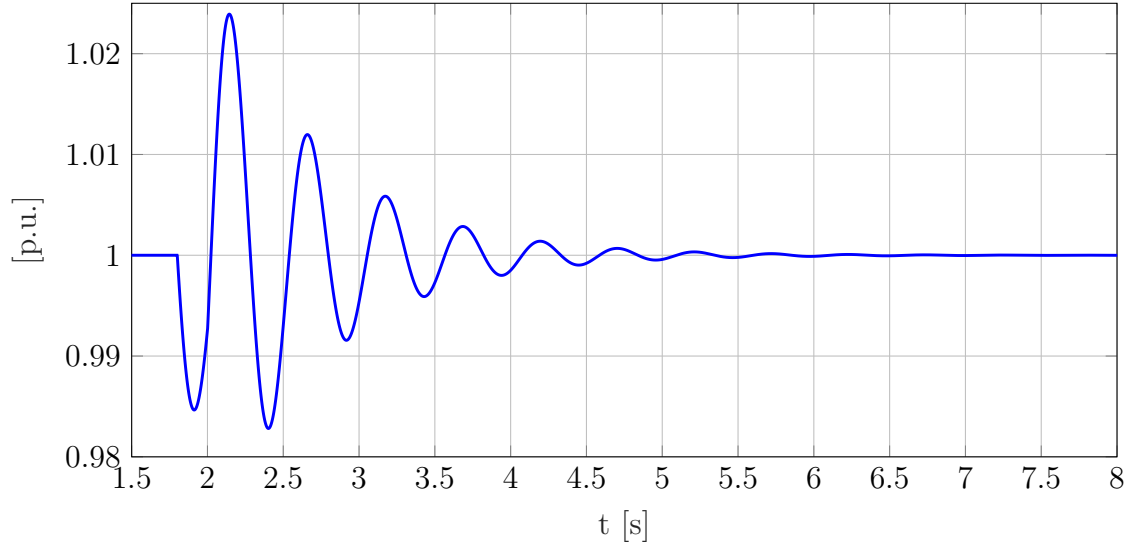


Figure 7: Rotor speed of the RFC, Case 1.

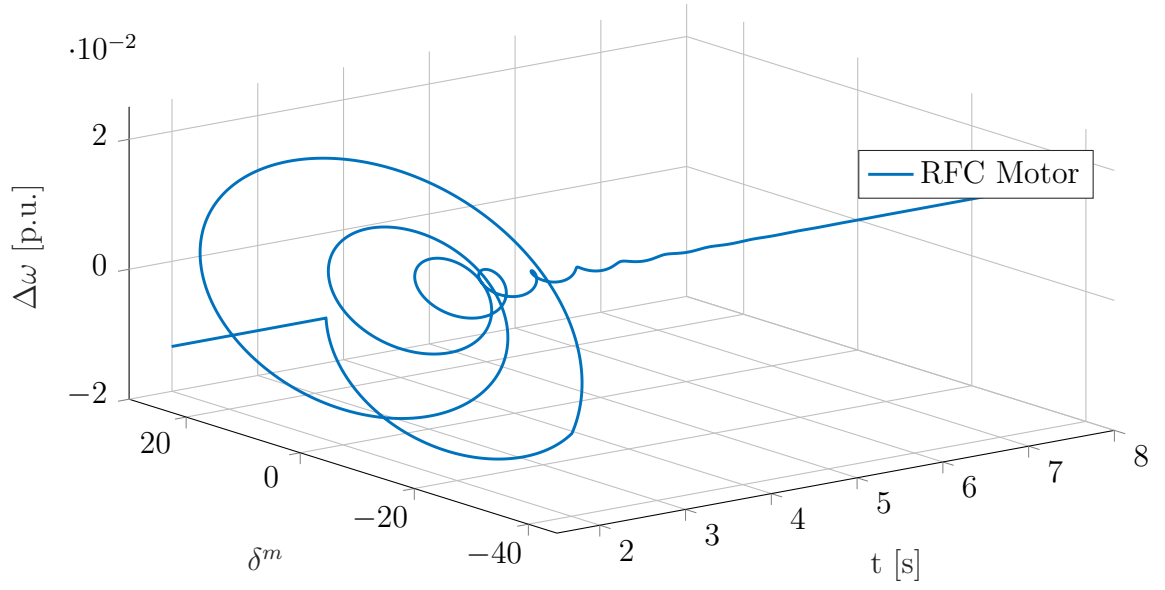


Figure 8: Phase plot δ^m vs $\Delta\omega_{p.u.}$ vs time, Case 1.

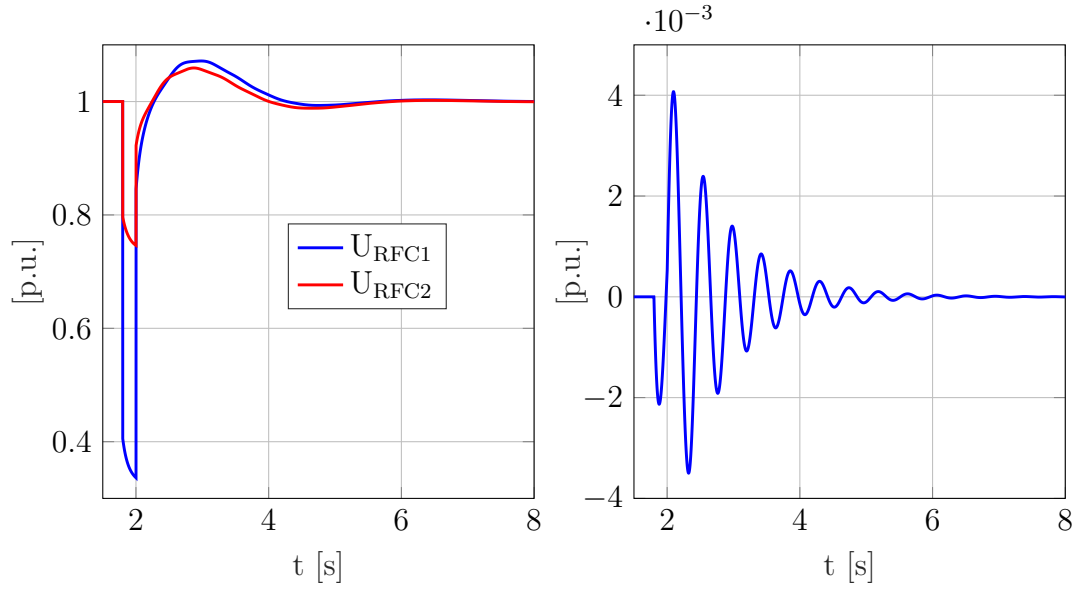
The simulations show that the rotor speed oscillation of RFC 1 and RFC 2 has an average frequency of 1.96 Hz as seen in Figure 9c. The three-phase powers will oscillate at 1.96 Hz for both RFC, see Figure 9d. This is in line with Case 1, as the both RFCs are of the same type.

The average frequency of the relative rotor oscillation, $\Delta\omega_{12} = \omega_{\text{RFC1}} - \omega_{\text{RFC2}}$, between the RFC in interconnected mode is about 2.27 Hz see Figure 9b. The single-phase power between the RFCs oscillates with same frequency, see Figures 10a and 10b.

Note that the average frequency of the single-phase active power oscillations differs from the three-phase active power oscillation. There are several reasons for the difference, such as the grid impedance of the railway grid, rotor angle difference between RFC single-phase generators, location of the fault and excitation system equipped on the single-phase generators.

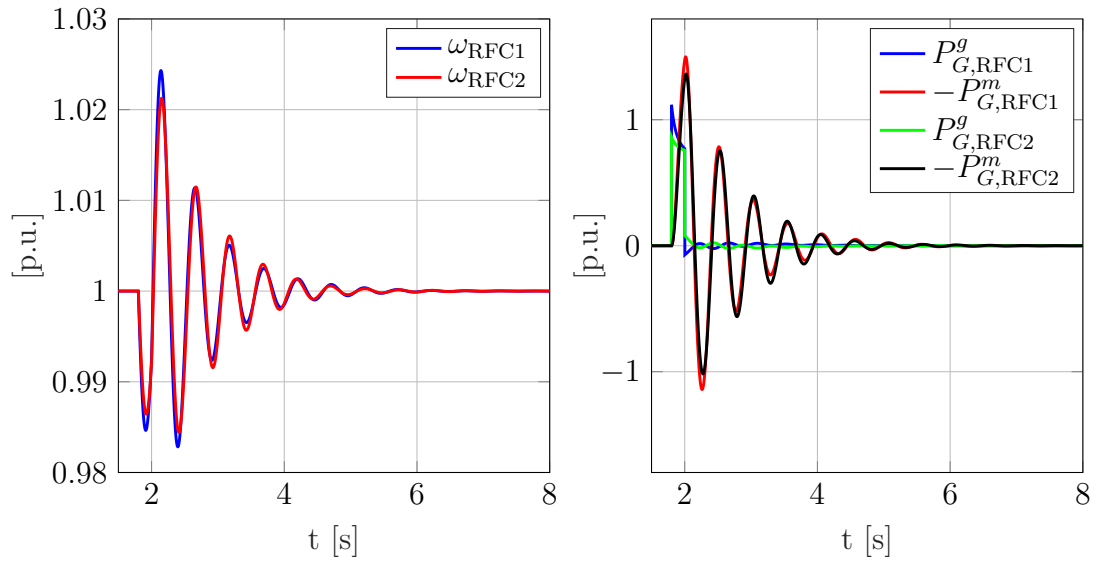
As in Case 1, the three-phase power consumed by each individual RFC motor lags the single-phase active power generated by the RFC generator, see Figure 9.

The simulation shows also that the reactive power oscillates with a frequency of approximately 2.45 Hz in the single-phase side, see Figures 10c and 10d.



(a) Voltage after the step-up transformer, railway side.

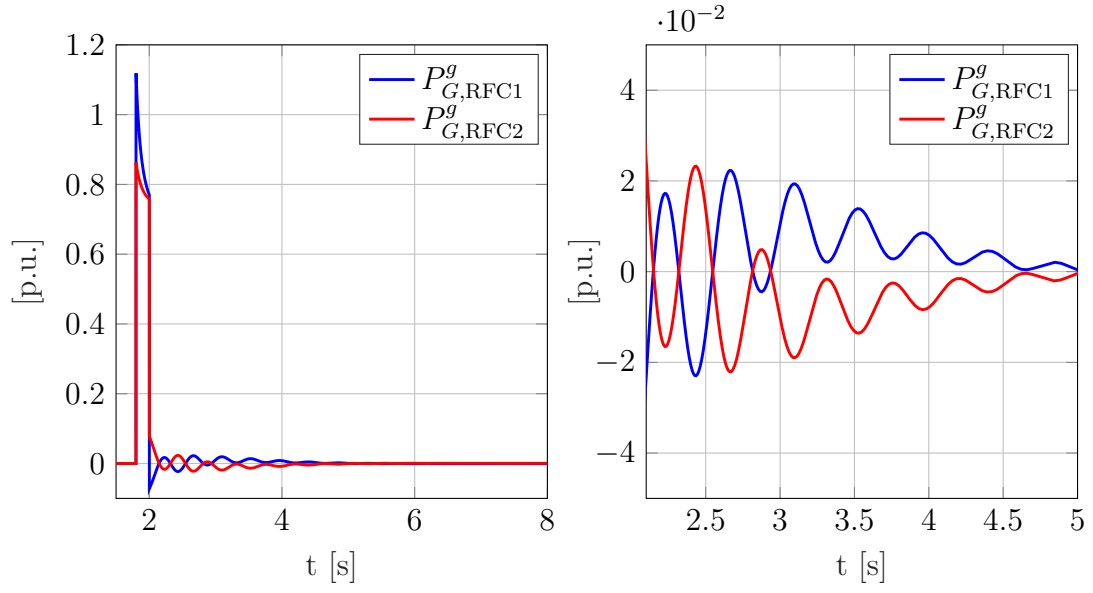
(b) Relative rotor speed between the RFCs.



(c) Rotor speeds of the RFCs.

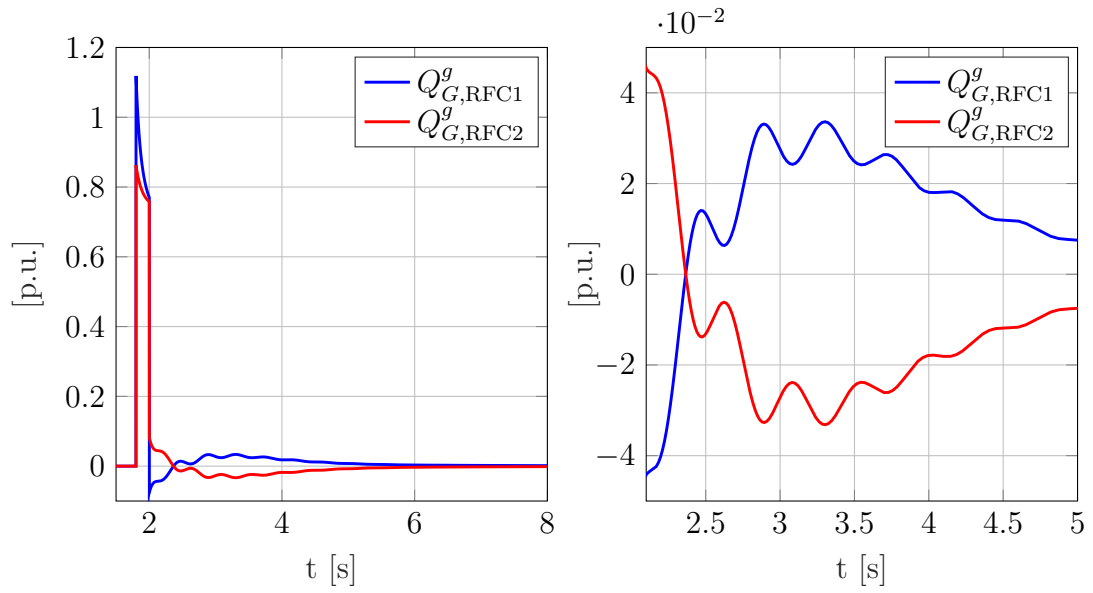
(d) Generated and consumed active power of the RFCs generator & motor.

Figure 9: Case 2 results.



(a) Active power.

(b) Zoom of active power.



(c) Reactive power.

(d) Zoom of reactive power.

Figure 10: Case 2 results of generated active and reactive power of each RFC's generator.

6. Conclusions

An open high order electromechanical dynamical model of an RFC has been developed by using well established synchronous machine models. The model is suited for electromechanical stability studies of low frequency railway grids that are synchronously connected to three-phase public grids.

Numerical studies in the phasor domain have been performed, to graphically explain and illustrate the behaviour of the proposed RFC model, using data for one of the most common RFC models (the Q48/Q49) used in Sweden. The case studies include both single feeding of a catenary section and two-sided catenary feeding (that is, the simplest way that a railway power system can be operating in interconnected mode). The two basic cases of feeding a railway together facilitates illustrating many important aspects of the RFC behaviour in simple manners. From the modelling and the case studies done, it can be concluded that the three-phase active power lags the single-phase active power, in line with [8], as the inertia of the RFC will cause a time delay.

The model presented could be used for electro-magnetic transient (EMT) simulations with proper adaptations, depending on the desired level of details. However, going into deeper details may be a complicated task, specially how to adapt the electrical machine equations for the single-phase salient pole generator. The reader should note, that single-phase powers (active as well as reactive), unlike three-phase powers, are not constant even in steady-state operation. Single-phase power oscillates with twice the grid frequency.

The open models presented in this work constitute an important step in the work for ensuring the future reliability and stability of low-frequency rail-

ways, an important societal asset. The high order RFC model in this paper is the first of its kind presented in the academic literature. Its implementation for stability studies done in this paper provide an open starting platform, which can be used for education and future research of low-frequency railway grids synchronously connected to three-phase public grids.

References

- [1] Steimel A. Power-electronic grid supply of AC railway systems. In: 2012 13th International Conference on Optimization of Electrical and Electronic Equipment (OPTIM). IEEE. ISBN 978-1-4673-1653-8; 2012, p. 16–25. URL <http://ieeexplore.ieee.org/lpdocs/epic03/wrapper.htm?arnumber=6231844>.
- [2] Steimel A. Electric Traction - Motive Power and Energy Supply. Munich: Oldenbourg Industrieverlag GmbH; 2008.
- [3] Pfeiffer A, Scheidl W, Eitzmann M, Larsen E. Modern rotary converters for railway applications. In: Proceedings of the 1997 IEEE/ASME Joint Railroad Conference. IEEE. ISBN 0-7803-3854-5; 1997, p. 29–33. URL <http://ieeexplore.ieee.org/lpdocs/epic03/wrapper.htm?arnumber=581349>.
- [4] Zynovchenko A, Haubrich HJ, Treige P. Converter control and stability of the 110-kV railway grid increasing use of the static frequency converters. In: 2005 European Conference on Power Electronics and Applications. IEEE. ISBN 90-75815-09-3; 2005, p. 8 pp.–

- P.8. URL <http://ieeexplore.ieee.org/lpdocs/epic03/wrapper.htm?arnumber=1665449>.
- [5] Danielsen S, Fosso OB, Molinas M, Suul JA, Toftevaag T. Simplified models of a single-phase power electronic inverter for railway power system stability analysis - Development and evaluation. *Electric Power Systems Research* 2010;80(2):204–14. URL <http://linkinghub.elsevier.com/retrieve/pii/S0378779609002065><http://www.sciencedirect.com/science/article/pii/S0378779609002065>.
 - [6] Danielsen S, Molinas M, Toftevaag T, Fosso OB. Constant power load characteristic's influence on the low-frequency interaction between advanced electrical rail vehicle and railway traction power supply with rotary converters. In: *Modern electric traction (MET)*. Warsaw, Poland; 2009,.
 - [7] Danielsen S, Fosso OB, Toftevaag T. Use of participation factors and parameter sensitivities in study and improvement of low-frequency stability between electrical rail vehicle and power supply. In: *13th European Conference on Power Electronics and Applications*. 2009, p. 1–10. URL <http://ieeexplore.ieee.org/document/5279188/>.
 - [8] Danielsen S. *Electric Traction Power System Stability*. Ph.D. thesis; Norwegian University of Science and Technology; 2010.
 - [9] Eitzmann M, Paserba J, Undrill J, Amicarella C, Jones A, Khalafalla E, et al. Model development and stability assessment of the Amtrak 25 Hz traction system from New York to Washington DC. In: *Proceedings of*

- the 1997 IEEE/ASME Joint Railroad Conference. IEEE. ISBN 0-7803-3854-5; 1997, p. 21–8. URL <http://ieeexplore.ieee.org/lpdocs/epic03/wrapper.htm?arnumber=581348>.
- [10] Olofsson M. Undersökning av transient stabilitet i matningssystem för elektrisk tågdrift/Investigations of transient stability in railway power supply. Master thesis; KTH; 1989.
 - [11] Machowski J, Bialek JW, Bumby JR. POWER SYSTEM DYNAMICS - Stability and Control. John Wiley & Sons, Ltd; second ed.; 2008. ISBN 9780470725580.
 - [12] Milano F. Power System Modelling and Scripting. London: Springer; 2010. ISBN 9783642136689.
 - [13] Anderson P, Fouad A. Power System Control and Stability. Wiley-Interscience; second ed.; 2003.
 - [14] Olofsson M. Optimal Operation of the Swedish Railway Electrical System - An application of Optimal Power Flow. Ph.D. thesis; Royal Institute of Technology; 1996.
 - [15] Saadat H. Power System Analysis. PSA Publishing; third ed.; 2010.
 - [16] Laury J, Abrahamsson L, Bollen M. Modified voltage control law for low frequency railway power systems. In: Joint Rail Conference. Philadelphia: ASME; 2017,.
 - [17] Swedish Transport Administration . –. techreport TDOK 2013:0670; Swedish Transport Administration; 2013. Version 1.0.

- [18] IEEE . IEEE Recommended Practice for Excitation System Models for Power System Stability Studies; vol. 2005. 2006. ISBN 0738147869.
- [19] Dandeno P, Kundur P. A Non-Iterative Transient Stability Program Including the Effects of Variable Load-Voltage Characteristics. IEEE Transactions on Power Apparatus and Systems 1973;PAS-92(5):1478–84. URL <http://ieeexplore.ieee.org/document/4075237/>.
- [20] Cutsem TV, Vournas C. Voltage Stability of Electric Power Systems. Springer; 1998.
- [21] Abrahamsson L. Considering risks in power system operation and the consequences of different accepted risk levels. resreport REPORT 2017:375; Luleå University of Technology; Skellefteå, Sweden; 2017. DOI: 10.13140/RG.2.2.20511.66726; URL <https://energiforskmedia.blob.core.windows.net/media/23118/considering-risks-in-power-system-operation-energiforskrappport-2017-375.pdf>.
- [22] Kundur P. Power System Stability and Control. McGraw-Hill, Inc.; 1994.
- [23] Fridman E. Impedanser för/ Impedances KTL och 132 kV, 30 kV och 15 kV ML. Tech. Rep.; Trafikverket; 2006.
- [24] Abrahamsson L. Railway Power Supply Models and Methods for Long-term Investment Analysis. Licentiate thesis; KTH, Electric Power Systems; 2008.

- [25] GAMS Software GmbH. 2018. URL <https://www.gams.com>.
- [26] Basler M, Schaefer R. Understanding power system stability. In: 58th Annual Conference for Protective Relay Engineers, 2005. IEEE. ISBN 0-7803-8896-8; 2005, p. 46–67. URL <http://ieeexplore.ieee.org/document/1430421/>.
- [27] Rogers G. Power System Oscillations. New York: Springer Science & Buisness Media, LLC; 2000. ISBN 978-1-4613-7059-8.